Nonlinear Electronic Density Response in Warm Dense Matter

Dornheim, T.; Vorberger, J.; Bonitz, M.;

Originally published:

August 2020

Physical Review Letters 125(2020)8, 085001

DOI: https://doi.org/10.1103/PhysRevLett.125.085001

Nonlinear Electronic Density Response in Warm Dense Matter

Tobias Dornheim,[1,*] Jan Vorberger,[2] and Michael Bonitz[3]
[1]Center for Advanced Systems Understanding (CASUS), D-028262 Görlitz, Germany
[2]Helmholtz-Zentrum Dresden-Rossendorf, Bautzner Landstraße 400, D-01328 Dresden, Germany
[3]Institut für Theoretische Physik und Astrophysik, Christian-Albrechts-Universität zu Kiel, Leibnizstraße 15, D-24098 Kiel, Germany

(Received 9 April 2020; accepted 20 July 2020; published 19 August 2020)

Warm dense matter (WDM)—an extreme state with high temperatures and densities that occurs, e.g., in astrophysical objects—constitutes one of the most active fields in plasma physics and materials science. These conditions can be realized in the lab by shock compression or laser excitation, and the most accurate experimental diagnostics is achieved with lasers and free electron lasers which is theoretically modeled using linear response theory. Here, we present first *ab initio* path integral Monte Carlo results for the nonlinear density response of correlated electrons in WDM and show that for many situations of experimental relevance nonlinear effects cannot be neglected.

DOI: 10.1103/PhysRevLett.125.085001

Warm dense matter (WDM) is an exotic state with extreme densities ($r_s = \bar{r}/a_B \sim 1$ with $\bar{r}$ and a_B being the average inter-electron distance and first Bohr radius) and high temperatures ($\theta = k_B T/E_F \sim 1$ with T and E_F being the temperature and Fermi energy) that occurs, e.g., in astrophysical objects [1–4] on timescales of 10^6 years, in laser-excited solids [5,6] over femto- to picoseconds, and on the pathway towards inertial confinement fusion [7] over nano- to microseconds. Consequently, WDM has emerged as one of the most active frontiers in plasma physics and material science [8–10], and WDM conditions are routinely realized in experiments in large research facilities around the globe (e.g., NIF, SLAC, and the European XFEL); see Refs. [11–13] for review articles.

On the other hand, the theoretical description of WDM constitutes a formidable challenge [14,15] due to the complicated interplay of (i) Coulomb coupling, (ii) thermal excitations, and (iii) electronic quantum degeneracy effects. Moreover, the bulk of WDM theory assumes a weak response of the electrons to an external perturbation, i.e., they rely on linear response theory (LRT). This assumption enters, for example, in the interpretation of XRTS experiments [9,16], the characterization of the stopping power in WDM [17], the construction of effective potentials [18–20], density functional theory (DFT) calculations [21,22], and the computation of energy relaxation rates [6,23,24]. Consequently, numerous works have been devoted to the description of the density response of electrons both in the ground state [25–34] and at finite temperature [35–43]. These efforts have culminated in the recent machine-learning representation [44] of the static electronic density response that is based on *ab initio* path integral Monte Carlo (PIMC) simulations [45–47] and covers the entire WDM regime. Moreover, even the dynamic density response can be computed from PIMC simulations [48,49], and the reported negative dispersion relation of a uniform electron gas (UEG) constitutes an active topic of investigation.

On the other hand, very little is known about the density response of correlated electrons beyond the linear regime. In particular, it is unclear up to which perturbation strength LRT remains accurate. This question becomes increasingly urgent, as free electron lasers become more powerful and peak intensities of up to $I \sim 10^{22}$ W/cm^2 [50] have been reported. Furthermore, intense VUV lasers are used to probe WDM [51]. A particular promising tool is THz lasers [52] as they allow for probing the low-frequency end of the density response, short pulse characterization, and streaking [53–55]. Yet, THz field applications might require in many cases a theoretical description beyond LRT, as we indicate below.

In this work, we go beyond linear response theory by carrying out extensive PIMC simulations of a harmonically perturbed electron gas [41,42] [cf. Eq. (1) below] at WDM conditions. This allows us to measure the actual density response of the electrons without any *a priori* assumptions and, thus, to unambiguously characterize the validity range of LRT. In addition, going beyond the linear regime allows us to gauge the systematic errors of LRT as a function of perturbation strength, and to report the first results for the cubic response function $\chi_3(q)$ over the entire relevant wave number range for different densities and temperatures including all exchange-correlation effects. Therefore, our results provide the basis for a generalized theory of the electronic density response beyond LRT, extending earlier work for classical plasmas [56,57] and moderately coupled quantum plasmas [58,59].

Our investigation of the nonlinear density response of electrons in WDM should be relevant for many other fields, and spark similar investigations in other domains as we note that LRT is one of the most successful concepts in physics [60,61]. It is of paramount importance in many fields, such as for describing phonons in solid state physics [62,63], excitations in systems of ultracold atoms [64,65], and screening or quasiparticle excitations in plasmas [66,67]. Moreover, it has allowed for profound physical insights into, e.g., superfluidity [65,68], collective excitations [25,69], and quantum dynamics [21,70].

Results.—We simulate a harmonically perturbed electron gas of system size N governed by the Hamiltonian (we assume Hartree atomic units throughout this work)

$$\hat{H} = \hat{H}_{\mathrm{UEG}} + 2A\sum_{k=1}^{N}\cos\left(\hat{\mathbf{r}}_k\cdot\mathbf{q}\right), \tag{1}$$

with $\hat{H}_{\mathrm{UEG}}$ being the unperturbed UEG Hamiltonian [47,61,71], $\mathbf{r}_k$ the electronic coordinates, and the wave vector $\mathbf{q} = 2\pi/L(n_x, n_y, n_z)^T$ (with $n_i \in \mathbb{Z}$, and L being the length of the cubic simulation box). The perturbation amplitude A can, e.g., be the amplitude of an external electric field in the plasma or the modulation of the potential depth in an optical lattice [72]. Of particular relevance for WDM experiments is the realization of the modulation in Eq. (1) by a laser pulse; see Ref. [73] for details. We use a canonical adaption [80] of the worm algorithm by Boninsegni *et al.* [81,82] without any assumptions on the nodal structure of the thermal density matrix. Therefore, our simulations are computationally involved due to the fermion sign problem [83,84], but are exact within the given statistical uncertainty.

To measure the density response, we compute the induced density

$$\rho(\mathbf{q}, A) \coloneqq \langle\hat{\rho}_{\mathbf{q}}\rangle_A = \frac{1}{V}\left\langle\sum_{k=1}^{N} e^{-i\mathbf{q}\cdot\hat{\mathbf{r}}_k}\right\rangle_A, \tag{2}$$

where $\langle\ldots\rangle_A$ indicates the expectation value computed from Eq. (1). The PIMC results for Eq. (2) are shown in Fig. 1(a) as the green crosses for the electron gas with a metallic density ($r_s = 2$) at the Fermi temperature, $\theta = 1$, for a wave number of $q \approx 0.84 q_F$. First and foremost, we note that an increase in the perturbation strength leads to increasing deviations from a spatially homogeneous density profile, which, in turn, is measured by Eq. (2). For small A, LRT is accurate and it holds $\rho(\mathbf{q}, A) = \chi(\mathbf{q})A$, and the density response function $\chi(\mathbf{q})$ does not depend on A. Further, the linear response function can be computed from a simulation of the unperturbed UEG via the relation

$$\chi(\mathbf{q}) = -n\int_0^\beta d\tau F(\mathbf{q}, \tau), \tag{3}$$

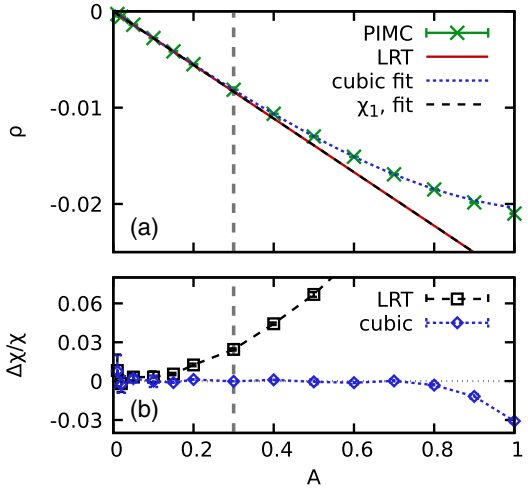

FIG. 1. Density response of the UEG for $N = 14$, $r_s = 2$, and $\theta = 1$ with $q \approx 0.84 q_F$ in dependence of the perturbation amplitude A [cf. Eq. (1)]. Panel (a) shows the PIMC data for the induced density ρ (green crosses), the prediction from LRT [solid red, cf. Eq. (3)], and a cubic fit [dotted blue, cf. Eq. (4)] as well as the linear component thereof (dashed black). Panel (b) shows the deviation of LRT (black squares) and the cubic fit (blue diamonds) from the PIMC data. The vertical gray dashed line corresponds to the maximum A value that has been included in the fit.

with $F(q, \tau)$ being the intermediate scattering function [9] evaluated at an imaginary time argument $\tau \in [0, \beta]$, see Ref. [44] for details. The LRT result for ρ as obtained from Eq. (3) is depicted by the solid red line and is in excellent agreement to the PIMC data for $A \lesssim 0.15$. This can be seen particularly well in Fig. 1(b), where the black squares correspond to the relative deviation between the PIMC data and LRT.

Yet, the system cannot react arbitrarily strongly with increasing A (this would lead to a *negative* density at the maxima of the external perturbation), and the response has to eventually saturate. Therefore, LRT systematically overestimates ρ, and the deviation to LRT appears to be parabolic in the depicted A range. Indeed, it is well known [31,32] that the first term beyond $\chi(q)$ is cubic in A and can be obtained by fitting the PIMC data to

$$\rho(\mathbf{q}, A) = \chi_1(q)A + \chi_3(q)A^3 + \cdots, \tag{4}$$

where $\chi_1(q)$ and $\chi_3(q)$ are the free parameters [85]. The results for Eq. (4) are included in Fig. 1(a) as the dashed blue curve, and exhibit a significantly improved agreement with the PIMC data as compared to LRT. The vertical dashed gray line corresponds to the maximum A value that has been included into the fit, but Eq. (4) remains accurate for significantly larger perturbation strengths, see also panel (b). For completeness, we mention that it is, in principle, redundant to obtain $\chi_1(q)$ from the PIMC data, as it is already known from Eq. (3). On the other hand,

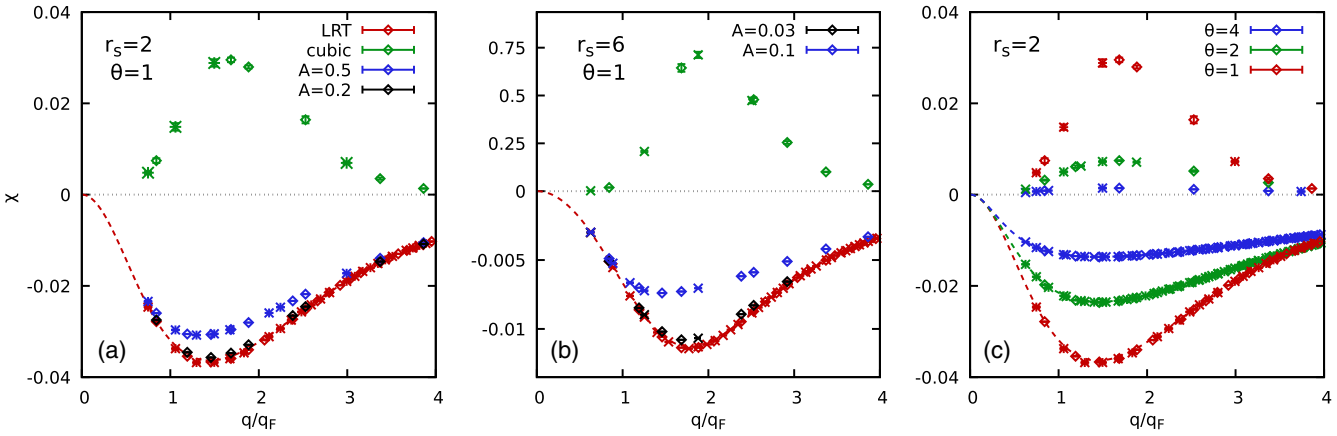

FIG. 2. Density response of an electron gas to an external harmonic perturbation at different conditions. Panels (a) and (b) show results for $\theta = 1$ and $r_s = 2$ and $r_s = 6$, respectively. The top halves correspond to the cubic response function $\chi_3(q)$ [computed via fits, cf. Eq. (4)], and the bottom half to the (pseudo-) linear response function $\chi(q)$ from LRT [red, cf. Eq. (3)], and for different perturbation amplitudes [black and blue, cf. Eq. (5)]. Panel (c) corresponds to $r_s = 2$ for $\theta = 4$ (blue), $\theta = 2$ (green), and $\theta = 1$ (red) and shows χ_3 and χ (from LRT) in the top and bottom half. The diamonds, stars, and crosses correspond to $N = 14$, 20, and 34. The dashed curves depict the LRT prediction computed from a recent machine-learning representation [44] of the static local field correction.

comparing the two allows to check the consistency of our approach, and the two independent estimations of the LRT function are in perfect agreement with an uncertainty interval of 0.1%, see the dashed black line in panel (a).

Let us next investigate the dependence of the response function on the wave number q. This is shown in Fig. 2(a) where the top and bottom half correspond to the cubic and linear response, respectively. The red symbols correspond to the usual LRT function computed from Eq. (3) for $N = 14$ (diamonds) and $N = 20$ (stars), and the dashed red line to $\chi(q)$ computed in the thermodynamic limit ($N \to \infty$) from the neural-net representation given in Ref. [44]. We note that they are in good agreement, as finite-size effects are small in this regime [44]. The black and blue symbols have been obtained from our new PIMC simulations of the perturbed system as

$$\chi(\mathbf{q}, A) = \frac{\rho(\mathbf{q}, A)}{A} \tag{5}$$

such that this *pseudo* response function converges to LRT in the limit of small perturbations, $\lim_{A\to 0}\chi(\mathbf{q}, A) = \chi(\mathbf{q})$. For $A = 0.2$ (black symbols), Eq. (5) is in good agreement to the LRT data both for small and large q, but systematically deviates around $q \sim q_F$. For $A = 0.5$ (blue symbols), the pseudo response function systematically underestimates the density response over the entire depicted q range, and the discrepancy is again most pronounced for intermediate wave numbers, with a maximum deviation of ~20%. To more systematically investigate this trend, we have performed extensive A scans such as depicted in Fig. 1 for different q values over the entire relevant wave number range [73]. This has allowed us to obtain the first results for the cubic response function $\chi_3(q)$, which are shown in the top half of Fig. 2(a) as the green data points. As a side note, we mention that a single $\chi_3(q)$ point requires 10–15 independent PIMC simulations of Eq. (1) with different A values for each wave number, which results in a total computation cost of $\mathcal{O}(10^7)$ CPU hours.

Overall, $\chi_3(q)$ qualitatively somewhat mirrors $\chi(q)$, although with some pronounced differences. First and foremost, we find that no finite-size effects can be resolved within the given error bars, and the only difference between $N = 14$ and $N = 20$ is the different q grid [87,88]. Moreover, $\chi_3(q)$ always has the opposite sign of $\chi(q)$, as the system cannot react arbitrarily strong to the perturbation, and the response eventually saturates. While both the linear and the cubic response function vanish in the large- and small-q limits, this happens significantly sooner for the latter function. Heuristically, this can be understood as follows: for large q values, only single-particle effects contribute to the response, the system as a whole remains hardly affected, and LRT is sufficient; further, the response is suppressed by the perfect screening [89] in the small-q limit. Similarly, we have found that both LRT and the cubic theory remain valid for larger A in both of these cases; see also Ref. [73]. Lastly, we find that the maximum in $\chi_3(q)$ appears to be slightly shifted to larger q values compared to $\chi(q)$, see also panel (b) for the same trend at $r_s = 6$.

Let us next investigate the dependence of the cubic response on the density parameter r_s. To this end, we repeat our previous study for $r_s = 6$, and the results are shown in Fig. 2(b) for $\theta = 1$. While such low densities are not typical for WDM applications, they can be realized experimentally in hydrogen jets [51] and evaporation experiments, e.g., at the Sandia Z-machine [90–93]. On the other hand, these conditions are highly interesting from a theoretical

point of view, as electronic exchange-correlation effects are even more important due to the increased coupling strength [47,94,95].

First and foremost, we find that the nonlinear behavior of the density response appears for significantly smaller perturbation amplitudes as compared to $r_s = 2$, which is due to the different energy scales in the system [96]. For example, for $A = 0.1$ the actual response (blue symbols) is suppressed by around 30%, whereas hardly any effect would be noticed at the higher density in this case. Overall, both $\chi(q)$ and $\chi_3(q)$ exhibit a similar structure as for $r_s = 2$, but are somewhat more symmetric around the maximum at $q \approx 2q_F$. Moreover, $\chi_3(q)$ nearly vanishes for the smallest depicted q value (the leftmost green cross, corresponding to $N = 34$) and we find a value more than 2 orders of magnitude smaller than for $q = 2q_F$. Again, no system-size dependence of $\chi_3(q)$ can be resolved within the given confidence interval even for $N = 34$ electrons (crosses).

Another interesting question is how nonlinear effects are influenced by the temperature. To this end, we return to $r_s = 2$ for $\theta = 1$ (red), $\theta = 2$ (green), and $\theta = 4$ (blue) in Fig. 2(c). With increasing temperature, the linear response function monotonically decreases in magnitude as it is expected, see the bottom half. The same also holds for the cubic response function, where this trend is drastically more pronounced compared to $\chi(q)$. While the maximum in $\chi(q)$ is reduced by a factor of 3 upon going from $\theta = 1$ to $\theta = 4$, the cubic response is reduced by a factor of 20.

This behavior is further illustrated in Fig. 3, where we show the A dependence of the induced density for the three temperatures at $q \approx 1.69q_F$, i.e., around the maximum of the density response. The different symbols correspond to our PIMC data, and the dotted lines to the prediction from LRT, i.e., Eq. (3). There are two dominant trends: (i) the actual density response is smaller for large θ and (ii) LRT remains accurate for larger A.

Let us conclude this investigation by briefly touching upon the impact of our findings on state-of-the-art WDM experiments. A typical free electron laser with a frequency corresponding to a photon energy of 8 keV and an intensity of $I \sim 10^{17-19}$ W/cm^2 corresponds to an approximate perturbation amplitude on the order of $A \sim 10^{-5}$–10^{-3} (see the Supplemental Material [73] for details), which falls safely into the LRT regime even for low densities. On the other hand, intensities of up to $I = 10^{22}$ W/cm^2 have been reported recently by employing the novel seeding technique [50], which results in $A \sim 2$ and clearly violates the boundaries of LRT for both for $r_s = 2$ and $r_s = 6$. Even current VUV lasers like Flash are capable of reaching the nonlinear regime [51,73]. Another application of our findings concerns the experimental probing of the low-frequency response of WDM using THz lasers [52]. For example, the recently reported setup with an intensity of 600 kV/cm at around 1 THz leads to a perturbation amplitude of $A = 0.29$ Ha, such that a thorough theoretical interpretation of a corresponding scattering signal would most likely require us to take into account nonlinear effects.

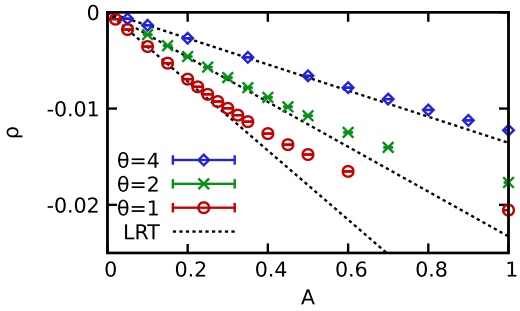

FIG. 3. Density response of the UEG for $N = 14$ and $r_s = 2$ with $q \approx 1.69q_F$ in dependence of the perturbation amplitude A [cf. Eq. (1)]. Shown are PIMC data for the induced density ρ for $\theta = 1$ (red circles), $\theta = 2$ (green crosses), and $\theta = 4$ (blue diamonds), as well as the corresponding predictions from LRT [dotted black, cf. Eq. (3)].

Summary.—We have carried out extensive *ab initio* PIMC simulations of the harmonically perturbed electron gas. This has allowed us to (i) unambiguously characterize the validity range of LRT and (ii) to obtain the first results for the cubic response function $\chi_3(q)$ of the warm dense electron gas, including all exchange-correlation effects. First, we have found that including $\chi_3(q)$ significantly improves the accuracy of the density response function for larger perturbation amplitudes. Moreover, nonlinear effects are particularly important for intermediate wave numbers $q \sim q_F$, whereas $\chi_3(q)$ vanishes both in the small- and large-q regimes. Regarding physical parameters, we have found that nonlinear effects become more important at lower densities due to the intrinsic energy scale of the system. This makes materials of relatively low density a highly interesting laboratory to study the interplay of nonlinearity with electronic exchange-correlation effects, and a challenging benchmark for theory.

In addition, we have found that nonlinear effects are severely affected by the electronic temperature and vanish upon increasing θ. While our current simulations are limited to temperatures down to the Fermi temperature ($\theta = 1$), this is a strong indication that nonlinear effects might be even more important for lower temperatures $\theta = 0.1 \ldots 0.5$, where many WDM experiments are located.

Our findings are particularly relevant for state-of-the-art WDM experiments with intense free electron lasers in the x-ray or VUV regime, and for low-frequency probing in the THz regime, where the diagnostics methods rely on theory input for the response functions [50–52]. Finally, our results will also be important for nonlinear optical diagnostics such as Raman or four-wave mixing spectroscopy, e.g., Refs. [97–99], or THz streaking [100] that could provide additional information on correlation effects in warm dense matter.

All PIMC data are available online [73] and can be used to benchmark approximate theories like DFT. Moreover, our new data are exact within the given confidence interval and thus provide the basis for a more general theory of the electronic density response beyond LRT thus further completing our understanding of the electron gas as a fundamental model system [47,101].

We acknowledge stimulating discussions with Richard Pausch and Dominik Kraus, and helpful comments by Michael Bussmann. This work was partly funded by the Center of Advanced Systems Understanding (CASUS) which is financed by Germany's Federal Ministry of Education and Research (BMBF) and by the Saxon Ministry for Science, Culture and Tourism (SMWK) with tax funds on the basis of the budget approved by the Saxon State Parliament, and by the Deutsche Forschungsgemeinschaft (DFG) via project BO1366/13. The PIMC calculations were carried out at the Norddeutscher Verbund für Hoch- und Höchstleistungsrechnen (HLRN) under Grant No. shp00015, on a Bull Cluster at the Center for Information Services and High Performace Computing (ZIH) at Technische Universität Dresden, on the clusters *hypnos* and *hemera* at Helmholtz-Zentrum Dresden-Rossendorf (HZDR), and at the computing center (Rechenzentrum) of Kiel university.

*t.dornheim@hzdr.de

[1] B. Militzer, W. B. Hubbard, J. Vorberger, I. Tamblyn, and S. A. Bonev, A massive core in jupiter predicted from first-principles simulations, Astrophys. J. **688**, L45 (2008).

[2] T. Guillot, Y. Miguel, B. Militzer, W. B. Hubbard, Y. Kaspi, E. Galanti, H. Cao, R. Helled, S. M. Wahl, L. Iess, W. M. Folkner, D. J. Stevenson, J. I. Lunine, D. R. Reese, A. Biekman, M. Parisi, D. Durante, J. E. P. Connerney, S. M. Levin, and S. J. Bolton, A suppression of differential rotation in Jupiter's deep interior, Nature (London) **555**, 227 (2018).

[3] D. Saumon, W. B. Hubbard, G. Chabrier, and H. M. van Horn, The role of the molecular-metallic transition of hydrogen in the evolution of Jupiter, saturn, and brown dwarfs, Astrophys. J. **391**, 827 (1992).

[4] A. Becker, W. Lorenzen, J. J. Fortney, N. Nettelmann, M. Schöttler, and R. Redmer, *Ab initio* equations of state for hydrogen (h-reos.3) and helium (he-reos.3) and their implications for the interior of brown dwarfs, Astrophys. J. Suppl. Ser. **215**, 21 (2014).

[5] R. Ernstorfer, M. Harb, C. T. Hebeisen, G. Sciaini, T. Dartigalongue, and R. J. D. Miller, The formation of warm dense matter: Experimental evidence for electronic bond hardening in gold, Science **323**, 1033 (2009).

[6] L. Waldecker, R. Bertoni, R. Ernstorfer, and J. Vorberger, Electron-Phonon Coupling and Energy Flow in a Simple Metal Beyond the Two-Temperature Approximation, Phys. Rev. X **6**, 021003 (2016).

[7] S. X. Hu, B. Militzer, V. N. Goncharov, and S. Skupsky, First-principles equation-of-state table of deuterium for inertial confinement fusion applications, Phys. Rev. B **84**, 224109 (2011).

[8] V. E. Fortov, Extreme states of matter on earth and in space, Phys. Usp. **52**, 615 (2009).

[9] S. H. Glenzer and R. Redmer, X-ray thomson scattering in high energy density plasmas, Rev. Mod. Phys. **81**, 1625 (2009).

[10] K. Falk, Experimental methods for warm dense matter research, High Power Laser Sci. Eng. **6**, e59 (2018).

[11] E. I. Moses, R. N. Boyd, B. A. Remington, C. J. Keane, and R. Al-Ayat, The national ignition facility: Ushering in a new age for high energy density science, Phys. Plasmas **16**, 041006 (2009).

[12] C. Bostedt, S. Boutet, D. M. Fritz, Z. Huang, H. J. Lee, H. T. Lemke, A. Robert, W. F. Schlotter, J. J. Turner, and G. J. Williams, Linac coherent light source: The first five years, Rev. Mod. Phys. **88**, 015007 (2016).

[13] T. Tschentscher, C. Bressler, J. Grnert, A. Madsen, A. P. Mancuso, M. Meyer, A. Scherz, H. Sinn, and U. Zastrau, Photon beam transport and scientific instruments at the european XFEL, Appl. Sci. **7**, 592 (2017).

[14] M. Bonitz, T. Dornheim, Z. A. Moldabekov, S. Zhang, P. Hamann, H. Khlert, A. Filinov, K. Ramakrishna, and J. Vorberger, *Ab initio* simulation of warm dense matter, Phys. Plasmas **27**, 042710 (2020).

[15] *Frontiers and Challenges in Warm Dense Matter*, edited by F. Graziani, M. P. Desjarlais, R. Redmer, and S. B. Trickey (Springer, International Publishing, New York, 2014).

[16] D. Kraus *et al.*, Characterizing the ionization potential depression in dense carbon plasmas with high-precision spectrally resolved x-ray scattering, Plasma Phys. Controlled Fusion **61**, 014015 (2019).

[17] W. Cayzac *et al.*, Experimental discrimination of ion stopping models near the bragg peak in highly ionized matter, Nat. Commun. **8**, 15693 (2017).

[18] G. Senatore, S. Moroni, and D. M. Ceperley, Local field factor and effective potentials in liquid metals, J. Non-Cryst. Solids **205**–**207**, 851 (1996).

[19] Z. A. Moldabekov, S. Groth, T. Dornheim, H. Kählert, M. Bonitz, and T. S. Ramazanov, Structural characteristics of strongly coupled ions in a dense quantum plasma, Phys. Rev. E **98**, 023207 (2018).

[20] Z. A. Moldabekov, H. Kählert, T. Dornheim, S. Groth, M. Bonitz, and T. S. Ramazanov, Dynamical structure factor of strongly coupled ions in a dense quantum plasma, Phys. Rev. E **99**, 053203 (2019).

[21] A. D. Baczewski, L. Shulenburger, M. P. Desjarlais, S. B. Hansen, and R. J. Magyar, X-ray Thomson Scattering in Warm Dense Matter Without the Chihara Decomposition, Phys. Rev. Lett. **116**, 115004 (2016).

[22] A. Pribram-Jones, P. E. Grabowski, and K. Burke, Thermal Density Functional Theory: Time-Dependent Linear Response and Approximate Functionals from the Fluctuation-Dissipation Theorem, Phys. Rev. Lett. **116**, 233001 (2016).

[23] J. Vorberger, D. O. Gericke, T. Bornath, and M. Schlanges, Energy relaxation in dense, strongly coupled two-temperature plasmas, Phys. Rev. E **81**, 046404 (2010).

[24] L. X. Benedict, M. P. Surh, L. G. Stanton, C. R. Scullard, A. A. Correa, J. I. Castor, F. R. Graziani, L. A. Collins,

O. Certík, J. D. Kress, and M. S. Murillo, Molecular dynamics studies of electron-ion temperature equilibration in hydrogen plasmas within the coupled-mode regime, Phys. Rev. E **95**, 043202 (2017).
[25] D. Bohm and A D. Pines, Collective description of electron interactions: II. Collective vs individual particle aspects of the interactions, Phys. Rev. **85**, 338 (1952).
[26] A. A. Kugler, Theory of the local field correction in an electron gas, J. Stat. Phys. **12**, 35 (1975).
[27] K. S. Singwi, M. P. Tosi, R. H. Land, and A. Sjölander, Electron correlations at metallic densities, Phys. Rev. **176**, 589 (1968).
[28] P. Vashishta and K. S. Singwi, Electron correlations at metallic densities V, Phys. Rev. B **6**, 875 (1972).
[29] A. Holas and S. Rahman, Dynamic local-field factor of an electron liquid in the quantum versions of the Singwi-Tosi-Land-Sjölander and Vashishta-Singwi theories, Phys. Rev. B **35**, 2720 (1987).
[30] B. Farid, V. Heine, G. E. Engel, and I. J. Robertson, Extremal properties of the harris-foulkes functional and an improved screening calculation for the electron gas, Phys. Rev. B **48**, 11602 (1993).
[31] S. Moroni, D. M. Ceperley, and G. Senatore, Static Response from Quantum Monte Carlo Calculations, Phys. Rev. Lett. **69**, 1837 (1992).
[32] S. Moroni, D. M. Ceperley, and G. Senatore, Static Response and Local Field Factor of the Electron Gas, Phys. Rev. Lett. **75**, 689 (1995).
[33] C. Bowen, G. Sugiyama, and B. J. Alder, Static dielectric response of the electron gas, Phys. Rev. B **50**, 14838 (1994).
[34] M. Corradini, R. Del Sole, G. Onida, and M. Palummo, Analytical expressions for the local-field factor $g(q)$ and the exchange-correlation kernel $K_{xc}(r)$ of the homogeneous electron gas, Phys. Rev. B **57**, 14569 (1998).
[35] S. Tanaka and S. Ichimaru, Thermodynamics and correlational properties of finite-temperature electron liquids in the Singwi-Tosi-Land-Sjölander approximation, J. Phys. Soc. Jpn. **55**, 2278 (1986).
[36] H. K. Schweng and H. M. Böhm, Finite-temperature electron correlations in the framework of a dynamic local-field correction, Phys. Rev. B **48**, 2037 (1993).
[37] F. Perrot and M. W. C. Dharma-wardana, Spin-polarized electron liquid at arbitrary temperatures: Exchange-correlation energies, electron-distribution functions, and the static response functions, Phys. Rev. B **62**, 16536 (2000).
[38] W. Stolzmann and M. Rösler, Static local-field corrected dielectric and thermodynamic functions, Contrib. Plasma Phys. **41**, 203 (2001).
[39] T. Sjostrom and J. Dufty, Uniform electron gas at finite temperatures, Phys. Rev. B **88**, 115123 (2013).
[40] S. Tanaka, Correlational and thermodynamic properties of finite-temperature electron liquids in the hypernetted-chain approximation, J. Chem. Phys. **145**, 214104 (2016).
[41] T. Dornheim, S. Groth, J. Vorberger, and M. Bonitz, Permutation blocking path integral Monte Carlo approach to the static density response of the warm dense electron gas, Phys. Rev. E **96**, 023203 (2017).
[42] S. Groth, T. Dornheim, and M. Bonitz, Configuration path integral Monte Carlo approach to the static density response of the warm dense electron gas, J. Chem. Phys. **147**, 164108 (2017).
[43] P. Arora, K. Kumar, and R. K. Moudgil, Spin-resolved correlations in the warm-dense homogeneous electron gas, Eur. Phys. J. B **90**, 76 (2017).
[44] T. Dornheim, J. Vorberger, S. Groth, N. Hoffmann, Z. A. Moldabekov, and M. Bonitz, The static local field correction of the warm dense electron gas: An ab initio path integral Monte Carlo study and machine learning representation, J. Chem. Phys. **151**, 194104 (2019).
[45] T. Dornheim, T. Sjostrom, S. Tanaka, and J. Vorberger, Strongly coupled electron liquid: Ab initio path integral monte carlo simulations and dielectric theories, Phys. Rev. B **101**, 045129 (2020).
[46] T. Dornheim, Z. A. Moldabekov, J. Vorberger, and S. Groth, *Ab initio* path integral Monte Carlo simulation of the uniform electron gas in the high energy density regime, Plasma Phys. Controlled Fusion **62**, 075003 (2020).
[47] T. Dornheim, S. Groth, and M. Bonitz, The uniform electron gas at warm dense matter conditions, Phys. Rep. **744**, 1 (2018).
[48] T. Dornheim, S. Groth, J. Vorberger, and M. Bonitz, Ab initio Path Integral Monte Carlo Results for the Dynamic Structure Factor of Correlated Electrons: From the Electron Liquid to warm Dense Matter, Phys. Rev. Lett. **121**, 255001 (2018).
[49] S. Groth, T. Dornheim, and J. Vorberger, Ab initio path integral Monte Carlo approach to the static and dynamic density response of the uniform electron gas, Phys. Rev. B **99**, 235122 (2019).
[50] L. B. Fletcher *et al.*, Ultrabright x-ray laser scattering for dynamic warm dense matter physics, Nat. Photonics **9**, 274 (2015).
[51] U. Zastrau *et al.*, Resolving Ultrafast Heating of Dense Cryogenic Hydrogen, Phys. Rev. Lett. **112**, 105002 (2014).
[52] B. K. Ofori-Okai, M. C. Hoffmann, A. H. Reid, S. Edstrom, R. K. Jobe, R. K. Li, E. M. Mannebach, S. J. Park, W. Polzin, X. Shen, S. P. Weathersby, J. Yang, Q. Zheng, M. Zajac, A. M. Lindenberg, S. H. Glenzer, and X. J. Wang, A terahertz pump mega-electron-volt ultrafast electron diffraction probe apparatus at the SLAC accelerator structure test area facility, J. Instrum. **13**, P06014 (2018).
[53] E. Goulielmakis, M. Uiberacker, R. Kienberger, A. Baltuska, V. Yakovlev, A. Scrinzi, T. Westerwalbesloh, U. Kleineberg, U. Heinzmann, M. Drescher, and F. Krausz, Direct measurement of light waves, Science **305**, 1267 (2004).
[54] U. Frühling, M. Wieland, M. Gensch, T. Gebert, B. Schütte, M. Krikunova, R. Kalms, F. Budzyn, O. Grimm, J. Rossbach, E. Plönjes, and M. Drescher, Single-shot terahertz-field-driven x-ray streak camera, Nat. Photonics **3**, 523 (2009).
[55] A. K. Kazansky, I. P. Sazhina, and N. M. Kabachnik, Angular streaking of auger-electrons by THz field, J. Phys. B **52**, 045601 (2019).
[56] K. I. Golden, F. Green, and D. Neilson, Nonlinear-response-function approach to binary ionic mixtures: Dynamical theory, Phys. Rev. A **32**, 1669 (1985).
[57] M. Bonitz, Z. Donkó, T. Ott, H. Kählert, and P. Hartmann, Nonlinear Magnetoplasmons in Strongly Coupled Yukawa Plasmas, Phys. Rev. Lett. **105**, 055002 (2010).

[58] N.-H. Kwong and M. Bonitz, Real-Time Kadanoff-Baym Approach to Plasma Oscillations in a Correlated Electron Gas, Phys. Rev. Lett. **84**, 1768 (2000).

[59] H. Haberland, M. Bonitz, and D. Kremp, Harmonics generation in electron-ion collisions in a short laser pulse, Phys. Rev. E **64**, 026405 (2001).

[60] W. Nolting and W. D. Brewer, *Fundamentals of Many-body Physics: Principles and Methods* (Springer, Heidelberg, 2009).

[61] G. Giuliani and G. Vignale, *Quantum Theory of the Electron Liquid* (Cambridge University Press, Cambridge, England, 2008).

[62] S. Baroni, P. Giannozzi, and A. Testa, Green's-Function Approach to Linear Response in Solids, Phys. Rev. Lett. **58**, 1861 (1987).

[63] S. Baroni, S. de Gironcoli, A. Dal Corso, and P. Gianozzi, Phonons and related crystal properties from density-functionalperturbation theory, Rev. Mod. Phys. **73**, 515 (2001).

[64] R. Haussmann, M. Punk, and W. Zwerger, Spectral functions and rf response of ultracold fermionic atoms, Phys. Rev. A **80**, 063612 (2009).

[65] E. L. Pollock and D. M. Ceperley, Path-Integral Computation of Superfluid Densities, Phys. Rev. B **36**, 8343 (1987).

[66] K. Nishikawa and M. Wakatani, *Plasma Physics: Basic Theory with Fusion Applications* (Springer Science & Business Media, Heidelberg, 2000).

[67] S. Ichimaru, Strongly coupled plasmas: High-density classical plasmas and degenerate electron liquids, Rev. Mod. Phys. **54**, 1017 (1982).

[68] D. M. Ceperley, Path integrals in the theory of condensed helium, Rev. Mod. Phys. **67**, 279 (1995).

[69] M. Bonitz, *Quantum Kinetic Theory* (Springer, Heidelberg, 2016).

[70] E. K. U. Gross and W. Kohn, Local Density-Functional Theory of Frequency-Dependent Linear Response, Phys. Rev. Lett. **55**, 2850 (1985).

[71] P.-F. Loos and P. M. W. Gill, The uniform electron gas, Comput. Mol. Sci. **6**, 410 (2016).

[72] A. Dirks, K. Mikelsons, H. R. Krishnamurthy, and J. K. Freericks, Theoretical description of coherent doublon creation via lattice modulation spectroscopy, Phys. Rev. A **89**, 021602(R) (2014).

[73] See Supplemental Material at http://link.aps.org/supplemental/10.1103/PhysRevLett.125.085001 for additional details, which includes Refs. [74–79].

[74] L. Brualla, K. Sakkos, J. Boronat, and J. Casulleras, Higher order and infinite trotter-number extrapolations in path integral monte carlo, J. Chem. Phys. **121**, 636 (2004).

[75] K. Sakkos, J. Casulleras, and J. Boronat, High order chin actions in path integral monte carlo, J. Chem. Phys. **130**, 204109 (2009).

[76] L. V. Keldysh, Ionization in the field of a strong electromagnetic wave, J. Exp. Theor. Phys. **20**, 1307 (1965).

[77] K. J. Schafer, B. Yang, L. F. DiMauro, and K. C. Kulander, Above Threshold Ionization Beyond the High Harmonic Cutoff, Phys. Rev. Lett. **70**, 1599 (1993).

[78] M. Lewenstein, P. Balcou, M. Y. Ivanov, A. L'Huillier, and P. B. Corkum, Theory of high-harmonic generation by low-frequency laser fields, Phys. Rev. A **49**, 2117 (1994).

[79] All PIMC raw data for the density response are freely available at https://doi.org/10.14278/rodare.409.

[80] F. Mezzacapo and M. Boninsegni, Structure, superfluidity, and quantum melting of hydrogen clusters, Phys. Rev. A **75**, 033201 (2007).

[81] M. Boninsegni, N. V. Prokofev, and B. V. Svistunov, Worm algorithm and diagrammatic Monte Carlo: A new approach to continuous-space path integral Monte Carlo simulations, Phys. Rev. E **74**, 036701 (2006).

[82] M. Boninsegni, N. V. Prokofev, and B. V. Svistunov, Worm Algorithm for Continuous-Space Path Integral Monte Carlo Simulations, Phys. Rev. Lett. **96**, 070601 (2006).

[83] M. Troyer and U. J. Wiese, Computational Complexity and Fundamental Limitations to Fermionic Quantum Monte Carlo Simulations, Phys. Rev. Lett. **94**, 170201 (2005).

[84] T. Dornheim, Fermion sign problem in path integral Monte Carlo simulations: Quantum dots, ultracold atoms, and warm dense matter, Phys. Rev. E **100**, 023307 (2019).

[85] We note that an A^2 term in Eq. (4) would lead to a different absolute value of the density response for A and $-A$, which is unphysical. Moreover, Eq. (4) constitutes an expansion around $A = 0$ and will break down when the external field becomes dominant. Finally, we mention the possible impact of harmonic contributions in the nonlinear regime, e.g., Ref. [86].

[86] M. Bonitz, D. C. Scott, R. Binder, and S. W. Koch, Nonlinear carrier-plasmon interaction in a one-dimensional quantum plasma, Phys. Rev. B **50**, 15095 (1994).

[87] T. Dornheim, S. Groth, T. Sjostrom, F. D. Malone, W. M. C. Foulkes, and M. Bonitz, Ab initio Quantum Monte Carlo Simulation of the Warm Dense Electron Gas in the Thermodynamic Limit, Phys. Rev. Lett. **117**, 156403 (2016).

[88] T. Dornheim, S. Groth, and M. Bonitz, *Ab initio* results for the static structure factor of the warm dense electron gas, Contrib. Plasma Phys. **57**, 468 (2017).

[89] A. A. Kugler, Bounds for some equilibrium properties of an electron gas, Phys. Rev. A **1**, 1688 (1970).

[90] J. F. Benage, W. R. Shanahan, and M. S. Murillo, Electrical Resistivity Measurements of Hot Dense Aluminum, Phys. Rev. Lett. **83**, 2953 (1999).

[91] V. V. Karasiev, L. Calderin, and S. B. Trickey, Importance of finite-temperature exchange correlation for warm dense matter calculations, Phys. Rev. E **93**, 063207 (2016).

[92] S. Mazevet, M. P. Desjarlais, L. A. Collins, J. D. Kress, and N. H. Magee, Simulations of the optical properties of warm dense aluminum, Phys. Rev. E **71**, 016409 (2005).

[93] M. P. Desjarlais, J. D. Kress, and L. A. Collins, Electrical conductivity for warm, dense aluminum plasmas and liquids, Phys. Rev. E **66**, 025401(R) (2002).

[94] S. Groth, T. Dornheim, T. Sjostrom, F. D. Malone, W. M. C. Foulkes, and M. Bonitz, Ab initio Exchange-Correlation Free Energy of the Uniform Electron Gas at Warm Dense Matter Conditions, Phys. Rev. Lett. **119**, 135001 (2017).

[95] K. Ramakrishna, T. Dornheim, and J. Vorberger, Influence of finite temperature exchange-correlation effects in hydrogen, Phys. Rev. B **101**, 195129 (2020).

[96] In fact, the kinetic and interaction energy of the unperturbed system scales (in first order) as $K \sim r_s^{-2}$ and $V \sim r_s^{-1}$, respectively. Yet, defining a rescaled perturbation amplitude [e.g., $\delta = A/(K+V)$] does not significantly simplify.

[97] N. Bloembergen, Nonlinear optics and spectroscopy, Rev. Mod. Phys. **54**, 685 (1982).

[98] S. Mukamel and R. F. Loring, Nonlinear response function for time-domain and frequency-domain four-wave mixing, J. Opt. Soc. Am. B **3**, 595 (1986).

[99] V. M. Axt and S. Mukamel, Nonlinear optics of semiconductor and molecular nanostructures; a common perspective, Rev. Mod. Phys. **70**, 145 (1998).

[100] B. Schütte, S. Bauch, U. Frühling, M. Wieland, M. Gensch, E. Plönjes, T. Gaumnitz, A. Azima, M. Bonitz, and M. Drescher, Evidence for Chirped Auger-Electron Emission, Phys. Rev. Lett. **108**, 253003 (2012).

[101] V. V. Karasiev, S. B. Trickey, and J. W. Dufty, Status of free-energy representations for the homogeneous electron gas, Phys. Rev. B **99**, 195134 (2019).